A Novel Unsupervised Approach for Land Classification Based on Touzi Scattering Vector Model in the Context of Very High Resolution PolSAR Imagery

Jian Gong, Sheng Sun, and Zhijia Xu

***Abstract*—With the popularization of very high resolution polarimetric synthetic aperture radar image dataset, it is essential to re-investigate the classification scheme for 2-D land cases. The Touzi scattering vector model, a unique and roll-invariant decomposition solution, is employed to extract the scattering properties of different land covers. The parameters of Touzi decomposition act as input dataset for initial classification. A novel classifying algorithm is put forward by means of integrating the Touzi decomposition with conventional Wishart statistical models. Quantitative experiments are then conducted using uninhabited aerial vehicle synthetic aperture radar sample data for evaluating the performance of this new proposed approach. It can be concluded from the experimental results that the new proposed method is superior to the classical method in terms of producer accuracy, user accuracy, and overall accuracy.**

***Index Terms*—Polarimetric synthetic aperture radar, scattering vector model, Touzi decomposition, unsupervised classification, very high resolution**

Original Research Paper
DOI: 10.7251/ELSxxxxxxxx

I. Introduction

LAND classification applications based on the polarimetric synthetic aperture radar (PolSAR) remain hotspots in the community of radar remote sensing over the past few decades. Classification methods play a prominent role in these applications. In general, these methods can be categorized into three groups: algorithms based on statistical models, algorithms based on physical scattering mechanisms, and the ones that combine both of them. The third group, on the whole, excels at this task owing to the combination of statistical and physical scattering characteristics [1]. For one thing, the manner in which physical scattering properties are extracted is of great importance to the classification of polarimetric synthetic aperture radar images. There were various academic explorations to deal with this problem in recent years. Kusano *et al.* in 2015 proposed a generalized scattering model based on the particle cloud model adding the ellipticity angle. Their experimental results showed that the decomposition parameters were considerably dissimilar from those of eigenvalue-based methods [2]. Besic *et al.* in 2015 put forward an alternative approach for polarimetric incoherent target decomposition (ICTD) that was dedicated to the analysis of very high resolution (VHR) polarimetric synthetic aperture radar images. They argued that this ICTD decomposition strategy was capable of retrieving the edge diffraction of an elementary trihedral by recognizing dipole as the second component [3]. Bhattacharya *et al.* in 2015 suggested an adaptive general four-component scattering power decomposition method that was an extension of the best-known Yamaguchi four-component decomposition [4]-[5]. Touzi *et al.* came up with a solution that was inspired from the Cloude-Pottier ICTD in 2016 [6]-[7]. They employed Kennaugh-Huynen scattering matrix con-diagonalization and derived a new scattering vector model (SVM). The symmetric scattering type (SST) was brought in by them for an unambiguous description of symmetric target scattering. Due to the limited space, it is unachievable to review all the related methods here. For another, researchers seek to apply these newly-developed polarimetric property extractors and statistical methods to land classification. Trisasongko presented an evaluation on strategies for rubber plantation mapping employing PolSAR data coupled with random forest and support vector machine in 2017. He showed that classification accuracy could be further augmented by integrating texture features [8]. Sonobe *et al.* conducted a classifying experiment using Sentinel-1A C-SAR images and the Sentinel-2A image acquired during the 2016 growing season. They demonstrated an overall classification accuracy of 96.8% by means of kernel-based extreme learning machine [9]. Middinti *et al.* argued that the integration of polarimetric information with textures could supply complimentary information in forest type discrimination and produce high accuracy map [10]. Ohki *et al.* accomplished a large-area land classification over entire Japan using PALSAR-2 data. They implemented an algorithm based on support vector

Manuscript received 6 March 2020. Received in revised form 27 May 2020. Accepted for publication 27 June 2020. This paper was supported in part by the Guangdong Ocean and Fisheries Bureau Science and Technology Plan Projects under Grant No. A201701D04 and the cooperation funds between Guiyang Technology Bureau and Guiyang University under Grant No. GYU-KYZ(2019~2020)JX-17.

Jian GONG is with the Guangzhou Railway Polytechnic, 100 Qinglong Middle Rd, Baiyun, Guangzhou, Guangdong Province, 510430, China. (e-mail: 33668933@qq.com).

Sheng SUN is with the Guangdong University of Technology, No. 100 Waihuan Xi Road, Guangzhou Higher Education Mega Center, Panyu District, Guangzhou, Guangdong Province, 510006, China. (phone: +86-20-39322279; fax: +86-20-39322279; e-mail: sunsheng@gdut.edu.cn).

Zhijia XU is with the Guiyang University, 103 Jianlongdong Rd, Nanming District, Guiyang, Guizhou, 550005, China. (e-mail: xzjbelinda@163.com).

machine. Their experiments involved full polarimetry (FP), compact polarimetry (CP), and dual polarimetry (DP) data. The maximum accuracy of 73.4% was attained with 15 full polarimetric features [11]. Buono *et al*. developed two unsupervised classification algorithms on the basis of Wishart models by integrating Freeman-Durden and Cloude-Pottier decomposition methods. They conducted a quantitative comparison between two classifying schemes using a fully polarimetric C-band dataset acquired by Radarsat-2 over the test site, the Yellow River Delta of China [12]. Khosravi *et al*. put forward two improved decision tree ensembles that were named balanced filter-based forest (BFF) and cost-sensitive filter-based forest (CFF). These tree ensembles were reported to be able to deal with imbalanced data problems. The performances of such two tree ensembles were evaluated using three airborne L-band PolSAR datasets acquired by AIRSAR, EMISAR, and UAVSAR [13]. Li and Zhang came up with a unified Huynen dichotomy by extending Huynen decomposition. This new algorithm provided a unified selection mechanism. Additionally, they presented a classification method based on scattering degree of preference. They evaluated this new classifier on the classic San Francisco Bay sample data provided by AIRSAR [14].

Still, it is worthwhile to start an exploration of classification techniques based on the state-of-the-art polarimetric extractors in the context of very high resolution PolSAR images. Studies on the data of the very high resolution synthetic aperture radar systems, such as F-SAR [15] and Uninhabited Aerial Vehicle Synthetic Aperture Radar (UAVSAR) [16], are booming recently. The imagery data with very high resolution generally has large dimension and is in single, dual, and full polarization configurations. The spatial resolution of these systems is often decimeter level and the dimension is on the order of ten to twenty thousand by ten to twenty thousand pixels [17]. The size of the resolution cell with reference to these very high resolution data is close to the radar wavelength. One fundamental presumption, for the fully developed speckle, is that the resolution cell is much larger than the radar wavelength. This presumption will become ineffective, because the diameter of the resolution cell is only about six to ten times larger than radar wavelength [17]. Hence, it is necessary to re-validate those classical statistical models for PolSAR data. Meanwhile, it is also essential to re-design and re-evaluate the algorithms for land classification using very high resolution PolSAR images.

In this paper, the Touzi scattering vector model is combined with statistical properties of SAR data. An unsupervised land classification scheme is implemented and applied to very high resolution PolSAR images. The experiment accomplished for land classification is one of the exploratory works on PolSAR images with decimeter-level resolution. The rest of this paper is organized as follows. An analysis for incoherent decomposition models for PolSAR will be put forth in Section II in the first place. Afterwards, we will describe the new proposed classification scheme based on Touzi incoherent decomposition model in Section III. A quantitative experiment using very high resolution PolSAR data will be conducted in Section IV. A brief summary will be drawn in the last section.

II. Analysis of Decomposition Models for PolSAR

A. Data for describing scattering medium

Most man-made and natural scatterers fall into two categories: deterministic scatterers and distributed scatterers. The former may be associated with a dominant and stable scattering phenomenon. Coherent target decompositions could be applied to the scattering matrix of imaging data and employed to characterize such sort of deterministic scattering targets, for extracting physical scattering properties. The latter corresponds to a medium that varies over time and is not stable or fixed. The radar scattering response of distributed scatterers consists of diverse scattering mechanisms. It is therefore only possible to extract the average physical scattering mechanism of these targets. Moreover, they will be affected by speckle to different degrees. These fluctuating targets can be described by the second order moment statistics of imaging data, such as coherency matrix or covariance matrix. The expression of scatter matrix S and coherency matrix T_3 are presented in equation (1) and (2) respectively. In the mono-static backscattering case, the scattering matrix is defined in terms of complex scattering coefficients of the observed medium. Its form can be cast in a local Cartesian basis for convenience. If the roles of the transmitting and receiving antennas are interchangeable, the reciprocity theorem goes into effect and then S_{XY} is equal to S_{YX}. The coherency matrix T_3 can be generated from the outer product of the target vector that is denoted by $\underline{k}$. The superscript T^* stands for conjugate transpose, while the operator <…> stands for temporal or spatial ensemble averaging in equation (2) [18].

$$S = \begin{bmatrix} S_{XX} & S_{XY} \\ S_{YX} & S_{YY} \end{bmatrix}, \underline{k} = \frac{1}{\sqrt{2}} \begin{bmatrix} S_{XX} + S_{YY} \\ S_{XX} - S_{YY} \\ 2S_{XY} \end{bmatrix} \tag{1}$$

$$T_3 = < kk^{T^*} > = \left\langle \begin{bmatrix} |k_1|^2 & k_1 k_2^* & k_1 k_3^* \\ k_2 k_1^* & |k_2|^2 & k_2 k_3^* \\ k_3 k_1^* & k_3 k_2^* & |k_3|^2 \end{bmatrix} \right\rangle = \left\langle \begin{bmatrix} T_{11} & T_{12} & T_{13} \\ T_{12}^* & T_{22} & T_{23} \\ T_{13}^* & T_{23}^* & T_{33} \end{bmatrix} \right\rangle \tag{2}$$

B. Decomposition Models for extracting polarimetric scattering properties

The purpose of target decomposition is to extract underneath scattering mechanisms as the sum of diverse pure scattering processes. Coherent target decomposition aims to express the measured scattering matrix S as a combination of a string of canonical scattering mechanisms. It is only suitable for deterministic targets. Incoherent target decomposition seeks to obtain the average scattering mechanism in each resolution cell and can merely be applied to distributed targets that are expressed in terms of coherency matrix or covariance matrix. Due to the limited space, it is impossible to review all the decomposition methods here. We will, in this paper, concentrate on Touzi scattering vector model which springs from Cloude-Pottier incoherent target decomposition. Cloude-Pottier incoherent target decomposition presented, to a certain extent, ambiguities of scattering

type parameter for some scatterers [7]. An example, listed in [7], showed that a helix scatterer and dihedral scatterer had identical Cloude-Pottier α scattering type parameter ($\alpha=\pi/2$). For this reason, these two distinct scatterers can not be distinguished by such a parameter. Touzi scattering vector model was put forth with the goal of solving such ambiguities [7].

Firstly, Touzi scattering vector model is derived by adopting a projection of the Kennaugh-Huynen scattering matrix con-diagonalization into the Pauli basis. This projection allows eliminating the aforementioned ambiguities. The Touzi scattering vector model is composed of one complex entity called symmetric scattering type (SST). This complex variable consists of symmetric scattering type magnitude α_s and phase $\phi_{\alpha s}$ which are defined in polar coordinates. The former one ranges from 0 to $\pi/2$ and the latter one ranges from $-\pi/2$ to $\pi/2$. These two parameters are defined as a function of the scattering matrix con-eigenvalues μ_1 and μ_2 in equation (3) [7]. Besides, the scattering vector model for symmetric and asymmetric targets is denoted as equation (4). m is the maximum amplitude return. φ is the orientation of the maximum polarization with respect to the horizontal polarization. τ_m and ψ correspond to the helicity and the absolute phase respectively.

$$\tan(\alpha_s)e^{j\phi_{\alpha s}} = \frac{\mu_1 - \mu_2}{\mu_1 + \mu_2} \tag{3}$$

$$\underline{e}^{SV} = m \mid \underline{e} \mid \exp(j\psi) \begin{bmatrix} 1 & 0 & 0 \\ 0 & \cos 2\varphi & -\sin 2\varphi \\ 0 & \sin 2\varphi & \cos 2\varphi \end{bmatrix} \begin{bmatrix} \cos\alpha_S \cos 2\tau_m \\ \sin\alpha_S \exp(j\phi_{\alpha S}) \\ -j\cos\alpha_S \sin 2\tau_m \end{bmatrix} \tag{4}$$

Secondly, it is required to extend the scattering vector model mentioned above on account of the fact that it can only be effective for deterministic targets. This extension can be implemented by means of the following three steps.

(1) Figure out the coherency matrix T_3 through a simple spatial averaging within a square window.

(2) Perform a diagonalization of coherency matrix T_3. The corresponding three eigenvectors u_i (i=1, 2, 3) and eigenvalues λ_i (i=1, 2, 3) will be obtained.

(3) Carry out the parametrization of three eigenvectors u_i (i=1, 2, 3) according to the scattering vector model in equation (4). Each eigenvector can be characterized in terms of scattering vector model basis-invariant parameters as equation (4). A process for extracting the average scattering mechanisms can be put into effect in the similar manner that Cloude-Pottier has utilized in [19]. The average scattering parameters can be obtained by applying an arithmetic mean to these eigenvectors and eigenvalues afterwards.

Lastly, the above extended scattering vector model is qualified to extract the physical scattering properties for both deterministic targets and distributed targets. It is notable that only symmetric scattering type magnitude α_s and phase $\phi_{\alpha s}$ are adequate to meet the demand for classifying a 2-D land. As a result, other parameters will be omitted in the following sections.

III. Classification algorithm based on Touzi Scattering Model

A. Statistical model for very high resolution PolSAR data

As far as very high resolution data is concerned, the size of the resolution cell is close to the radar wavelength. Many conventional statistical models are based on a fundamental assumption that the resolution cell is much larger than the radar wavelength. The diameter of the resolution cell of very high resolution PolSAR data is generally about six to ten times larger than radar wavelength. Such assumption may, therefore, become invalid with reference to most very high resolution PolSAR datasets, such as F-SAR and UAVSAR. The amplitudes of four fully polarimetric channels were investigated and their histograms were computed and shown in [20]. A tight fit of the Rayleigh distributions to these histograms can easily be observed. Furthermore, it can be concluded that Wishart distribution will still be correct for those very high resolution datasets [20]. For this reason, the statistical models based on Wishart probability distributions continue to be effective for classification scheme using very high resolution PolSAR datasets.

The distributions of n-look coherency matrix Z, defined in eqination (5), will be utilized here to extract physical scattering mechanisms using Touzi incoherent decomposition. For convenience, let $A=nZ$, then the matrix A follows a complex Wishart distribution. The matrix A is defined in eqination (6).

$$Z = \frac{1}{n}\sum_{i=1}^{n} \underline{k}(i)\underline{k}(i)^{T^*} \tag{5}$$

$$P_A^{(n)}(A) = \frac{|A|^{n-q}\exp(-Tr(T^{-1}A))}{K(n,q)|T|^n} \tag{6}$$

$$K(n,q) = \pi^{0.5q(q-1)}\Gamma(n),...,\Gamma(n-q+1)$$

The conventional Wishart distance, defined in equation (7), characterizes the distance between a pixel and a class. Such distance is essential to calculate the statistical distance for pixels. Let T_m denote the coherency matrix of a certain class center. It can be approximated by the averaging of all the training samples. Each pixel is labeled with a class code if its Wishart distance to this class is the minimum among all classes. In addition, it is requisite to bring up the distance between classes to split or merge classes. The so-called distance between class with label i and the one with label j is presented in equation (8).

$$d(Z,\omega_m) = \ln(|T_m|) + Tr(T_m^{-1}Z) \tag{7}$$

$$D_{ij} = \frac{1}{2}\{\ln(|T_i|) + \ln(|T_j|) + Tr(T_i^{-1}T_j + T_j^{-1}T_i)\} \tag{8}$$

B. Classification algorithm

In light of the analysis in Section II, Touzi incoherent target decomposition model is competent to extract physical scattering mechanisms unambiguously. For example, the symmetric scattering type phase $\phi_{\alpha s}$ has been proven to be effective for Convair-580 airborne dataset which has a resolution of 0.64 meter in azimuth and 5.6 meter in range direction [21]. This parameter could easily be used to produce a set of coarse classifying results. And an unsupervised classification scheme based on these coarse results is supposed to be convincing if it can be incorporated with conventional statistical assumptions. The core parameters of Touzi incoherent decomposition are the magnitude and phase of symmetric scattering type. These two parameters can collectively be used for describing symmetric and asymmetric targets. Moreover, they are not dependent on polarization basis of radar antennas because they are derived from eigenvalues that are polarimetric basis invariant. At last, they play a role similar to Cloude-Pottier incoherent decomposition in the process of producing initial input data for classification. It is remarkable that there are three other decomposition parameters in the original version of Touzi decomposition. They are nevertheless redundant in 2-D land classification applications and so that the new proposed algorithm will omit them for a lower computational complexity.

There are totally four types of land covers to be discerned, including vegetation, bare soil, urban area, and water body. The detailed steps of the proposed algorithm can be found in the following.

(1) Apply the Touzi incoherent target decomposition steps itemized in Section II. It has been investigated in [6] that the configurations of window size may introduce biases of decomposition parameters. These biases will introduce an amplified error in the final classification results. Due to the significant upgrading of spatial resolution of VHR PolSAR images, the requirement of 60-look processing window that corresponds to a 9*9 window size configuration, proposed in [6] and [7], should be loosened to gather nearly unbiased incoherent decomposition parameters. Alternatively, a 7*7 window size configuration will be deployed in this algorithm. The range of scattering type phase $\phi_{\alpha s}$ will be equally divided into eight sub sections, including $[-\pi/2, -3\pi/8]$, $[-3\pi/8, -2\pi/8]$, $[-2\pi/8, -\pi/8]$, $[-\pi/8, 0]$, $[0, \pi/8]$, $[\pi/8, 2\pi/8]$, $[2\pi/8, 3\pi/8]$, and $[3\pi/8, \pi/2]$. There will be eight initial top-level land classes correspondingly. Each pixel will be assigned a label according to their value of symmetric scattering type phase $\phi_{\alpha s}$.

(2) All the pixels in each top-level class will be sorted according to their symmetric scattering type magnitude α_s. The subsection with the highest 20% scattering type magnitude α_s for each top-level class and the subsection with the lowest 20% scattering type magnitude for its adjacent top-level class will be conflated to form a new second-level class. This step will generate fifteen second-level classes. Such tactic allows mitigating the negative effect of outliers in each top-level class.

(3) Adopt clustering for those second-level classes. Such clustering takes advantage of the conventional statistical models. The distance between classes in equation (8) will be employed in this step. The distance from one class to other classes will be calculated one after another. The classes with the lowest distance are merged into one class, *i.e.* the third-level class, and there will be four third-level classes ultimately. Each class center is generated by an averaging of all the members within this class.

(4) Traverse all the pixels in third-level classes. Re-calculate the Wishart distance between each pixel and each third-level class in light of equation (7). Then a re-assignment is performed for each pixel based on such a new distance. An iterative updating for class center is often needed for better classification accuracy.

(5) The new class center will be obtained by an average of all the pixels within this class in terms of scattering type phase. The mapping from third-level class to the actual land cover type is determined by equation (9). There will be four land cover types, including vegetation, bare soil, urban area, and water body. The last step is to allocate colors for each third-level class with the purpose of a better visualization.

$$third-level\ class = \begin{cases} \text{vegetation, if } -\pi/2 < \phi_{\alpha s} < -\pi/4 \\ \text{bare soil, if } -\pi/4 \le \phi_{\alpha s} < 0 \\ \text{urban area, if } 0 \le \phi_{\alpha s} < -\pi/4 \\ \text{water body, if } \pi/4 \le \phi_{\alpha s} < \pi/2 \end{cases} \tag{9}$$

The dataflow and flowchart of the new proposed algorithm are illustrated in Fig. 1 and Fig. 2, respectively.

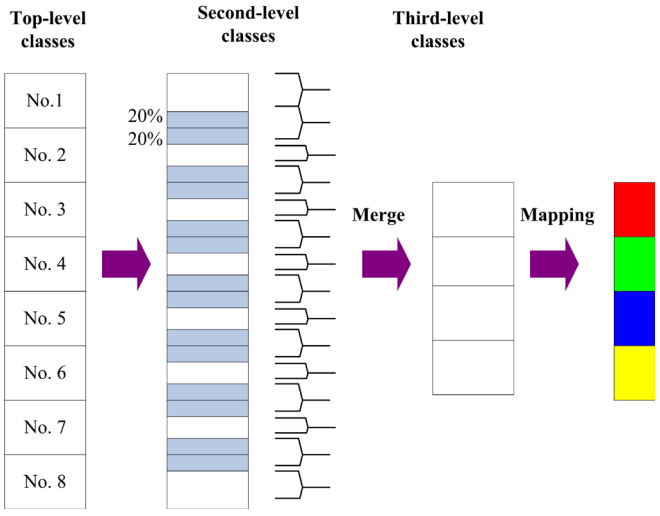

Fig. 1. The generating of top-level, second-level, and third-level classes and the dataflow.

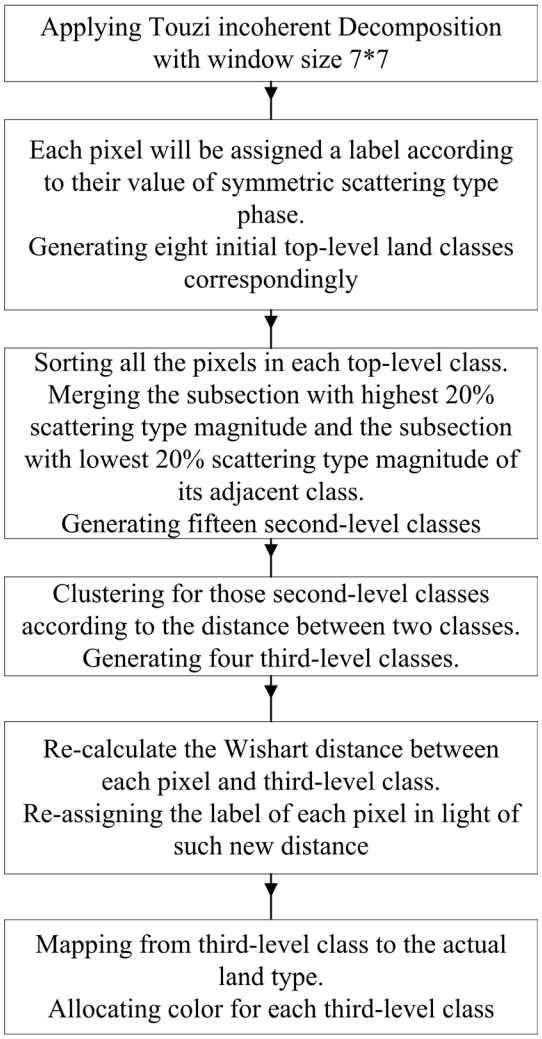

Fig. 2. The flowchart of classification scheme based on Touzi decomposition

IV. Experiment and Analysis

A. Test site and experimental data

The test site Rosario is the largest city in the province of Santa Fe, in central Argentina. It is located 300 km northwest of Buenos Aires, on the western shore of the Paraná River. It contains a lot of flat areas and represents a typical rural and urban landscape with heterogeneous land covers.

The very high resolution PolSAR experimental data to be evaluated is provided by the UAVSAR system. UAVSAR is a L-Band imaging radar instrument that uses microwaves in the 1.2 GHz range to detect and measure objects [16]. The detailed configurations of this original sample data are in table I. This sample data, courtesy of NASA/JPL-Caltech, is in single look complex (SLC) format and has slant range geometry. A sub-region with 2600 pixels in azimuth direction and 5772 pixels in range direction is cropped as an experimental area for the sake of low computational complexity. The Pauli coded pseudo-color image of this experimental area is presented in Fig. 4 (a). The production of ground truth map is accomplished under a commercial contract with Guangzhou Jiantong Surveying Mapping and Geo-information Technology Corporation, one Chinese A-class license survey company. This map for the land covers is obtained by annotations on the basis of the contemporaneous Google Earth imageries. It is essential to generate the plots of Cloude Pottier and Touzi Scattering Vector Model (TSVM) decomposition parameters respectively. These plots are listed in Fig. 3. Such plots are advantageous to make a visual comparison of the performance of two polarimetric decomposition methods. It can be easily seen from these plots that symmetric scattering type phase and magnitude attain better results for discerning diverse land covers.

Table I
The original experimental data and system configuration Parameters

Data ID:	rosari_16002 _15033_004_150402 _L090_CX_03	Acquisition Time:	April 2nd, 2015
Wavelength:	23.8403cm	Dimension of Azimuth:	93117
Dimension of Range:	9900	Size of cell in Azimuth and Range:	(0.6m, 1.66m)

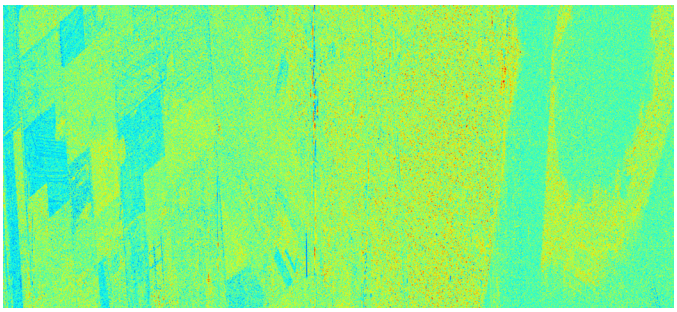

(a)

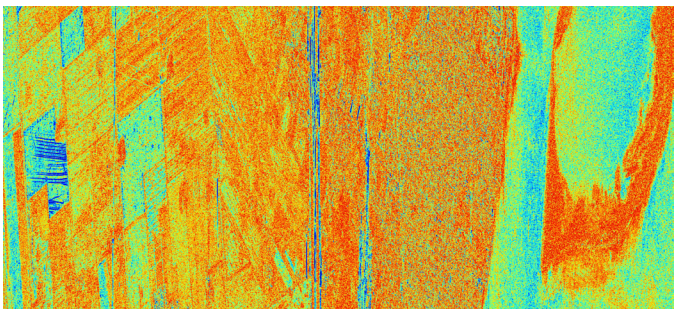

(b)

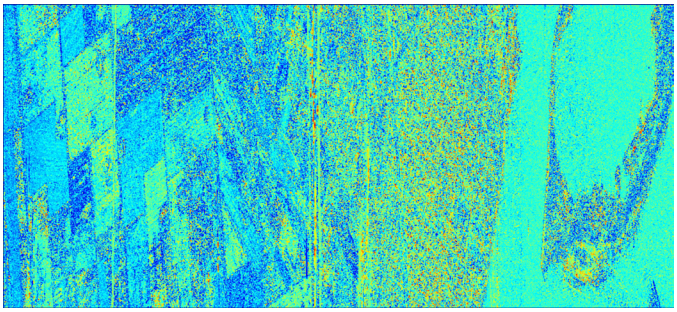

(c)

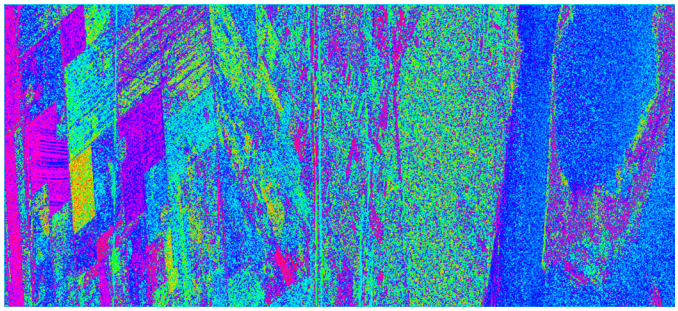

(d)

Fig. 3. The decomposition results of Cloude-Pottier target decomposition and TSVM decomposition: (a) Cloude-Pottier target decomposition - Alpha; (b) Cloude-Pottier target decomposition - Entropy; (c) TSVM decomposition - α_s ; (d) TSVM decomposition - $\phi_{\alpha s}$

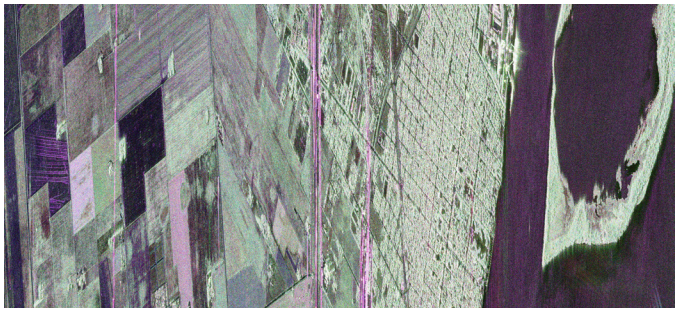

(a)

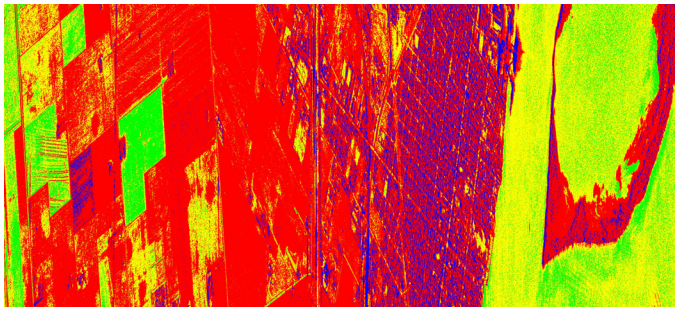

(b)

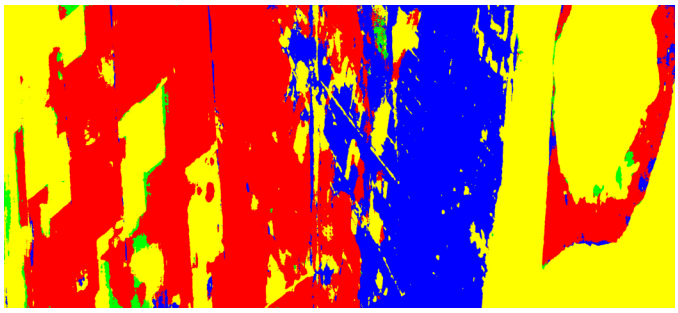

(c)

Fig. 4. (a) Pauli coded pseudo-color image of experimental area cropped from Rosario. UAVSAR data courtesy NASA/JPL-Caltech.
(b) Classification results using Cloude-Pottier Model; (c) Classification results using the new proposed method.

B. Evaluation Metrics

There are various evaluation metrics used in land cover classification. Due to the limited space, only three popular metrics, including user accuracy (*UA*), producer accuracy (*PA*), and overall accuracy (*OA*), will be involved in this study. Let *M* denote the total number of classes (*M*=4 in this study). Let C_{ij} denote the total number of pixels that actually belong to class *i* but are predicted to be class *j*. Then the user accuracy, producer accuracy, and overall accuracy are defined as equation (10), equation (11), and equation (12). The *UA* indicates the ratio of the pixels in a land cover that are correctly predicted to the pixels that are actually predicted to be such sort of cover. The *PA* signifies the proportion of pixels that are correctly predicted within a certain land cover to the total number of pixels of such land cover in ground truth data. *OA* suggests what proportion is correctly classified over all the classes.

$$UA_i = \frac{C_{ii}}{\sum_{j=1}^{M} C_{ji}} \tag{10}$$

$$PA_i = \frac{C_{ii}}{\sum_{j=1}^{M} C_{ij}} \tag{11}$$

$$OA = \frac{\sum_{i=1}^{M} C_{ii}}{\sum_{i=1}^{M}\sum_{j=1}^{M} C_{ij}} \tag{12}$$

C. Results and Analysis

A set of experiments will be conducted using the very high resolution sample data in Section IV. (A). The confusion matrix of two methods, Cloude-Pottier method and the new method based on TSVM, are presented in Table II and Table III, respectively. The corresponding predicting results are listed in Fig. 4 (b) and (c). The quantitative comparison in terms of *UA* and *PA* are illustrated in Fig. 5 and Fig. 6. It can be observed that the new method based on TSVM performs better than the one based on Cloude-Pottier decomposition model in general. The *UA* and *PA* of the new method for the urban area are significantly higher than the results obtained by the method based on Cloude-Pottier decomposition. These differences of performances are mainly caused by the ambiguity of Cloude-Pottier α scattering type parameter. The extent of improvement with respect to the classifying accuracy of bare soil is not so prominent compared with of other land covers. The relatively low accuracy for discerning bare soil is chiefly caused by the performance deficiency of TSVM in terms of bare soil. As to the overall accuracy, the method based on Cloude-Pottier decomposition only achieves 67.63%. In contrast, the new method proposed in this study reaches 80.99%. It is also worthwhile to make a comparison of other recent unsupervised or semi-unsupervised land classification algorithms for PolSAR imag-

eries. Actually, the quantitative results in different studies are acquired on diverse test data. Nevertheless, it will be helpful to introduce a quantitative comparison of their predicting accuracy taking into account the main parameters of the test data used by them. The Enhanced decision tree method proposed in [13] and a unified Huynen method proposed in [14] are involved in this comparison. The *OA* obtained by the classifiers based on Cloude-Pottier decomposition, new TSVM, Enhanced decision tree, and Unified Huynen decomposition on different test data are illustrated in Fig. 7. It can be observed that Enhanced decision tree and Unified Huynen method attain higher accuracy than the Cloude-Pottier method and our new proposed method. This is caused by the characteristics of test data. For one thing, the spatial resolution of test data Rosario is 2600×5772, but the test data Winnipeg and San Francisco are only 260×480 and 900×1024 respectively. For another, the test data Rosario covers a very large area with a lot of heterogeneous land objects. However, the test data Winnipeg and San Francisco cover a relatively small area with a large number of homogeneous land objects. The performance differences of the new proposed method are less than 7%, even though the current overall accuracy is obtained on a test data which corresponds to a much larger area. Furthermore, it will be meaningful to apply our new classifier to the classic PolSAR data, such as AIRSAR San Francisco image. The ground-truth annotations provided by Liu *et al.* are used to assess the performance of new TSVM classifier [22]. The original ground-truth data, however, have six classes, including unlabeled background, mountain, water body, urban, vegetation, and bare soil. To measure the accuracy in a fair setting, the background pixels are excluded from evaluation procedure. In addition, the class mountain and vegetation are merged into one class, *i.e.* vegetation. It is noteworthy that the metrics in [14] are not based on semantic classes but on the consistency of entropy/alpha classification plane. As a result, it is not suggested here to make a comparison of the performances of the two classifiers evaluated on the AIRSAR San Francisco data. The confusion matrix of TSVM classifier evaluated on the AIRSAR San Francisco data is presented in Table IV and the corresponding classification result is demonstrated in Fig. 8. It is well known that speckle effect becomes much more dominant with regard to SAR images with normal resolution. It can be seen that the speckle of San Francisco data decreases performance significantly. It should be noted that the total amount of pixels is only 802302 excluding background pixels.

TABLE II
CONFUSION MATRIX FOR LAND CLASSIFICATION BASED ON UNSUPERVISED CLOUDE-POTTIER DECOMPOSITION METHOD

	VE	BS	UR	WB	total	*PA*
VE	4511718	799145	377212	101963	5800038	*77.92%*
BS	564560	1311376	81932	287657	2245525	*58.40%*
UR	1484585	947728	1949323	83717	4465353	*43.65%*
WB	12123	104462	12549	2377150	2506284	*94.85%*
total	6582986	3162711	2421016	2850487	15007200	
UA	*68.69%*	*41.46%*	*80.52%*	*83.39%*		***67.63%***

TABLE III
CONFUSION MATRIX FOR LAND CLASSIFICATION BASED ON NEW PROPOSED METHOD

	VE	BS	UR	WB	total	*PA*
VE	4689992	754475	297754	47817	5790038	*81.00%*
BS	465617	1452614	76015	251279	2245525	*64.69%*
UR	694080	113791	3582009	75473	4465353	*80.22%*
WB	8658	56284	11024	2430318	2506284	*96.97%*
total	5858347	3086220	3257746	2804887	15007200	
UA	*80.06%*	*61.11%*	*90.30%*	*86.65%*		***80.99%***

TABLE IV
CONFUSION MATRIX FOR LAND CLASSIFICATION BASED ON TSVM METHOD EVALUATED ON SAN FRANCISCO DATA

	VE	BS	UR	WB	total	*PA*
VE	80688	15838	18695	1019	116240	*69.42%*
BS	860	11195	709	937	13701	*81.71%*
UR	101911	26947	213909	28	342795	*62.40%*
WB	95378	73093	10799	150296	329566	*45.60%*
total	278837	127073	244112	152280	802302	
UA	*28.94%*	*8.81%*	*87.63%*	*98.70%*		***56.85%***

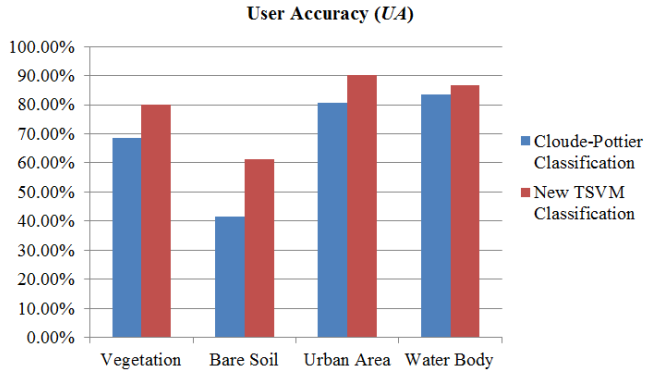

Fig. 5. *UA* of two classification methods over four land covers

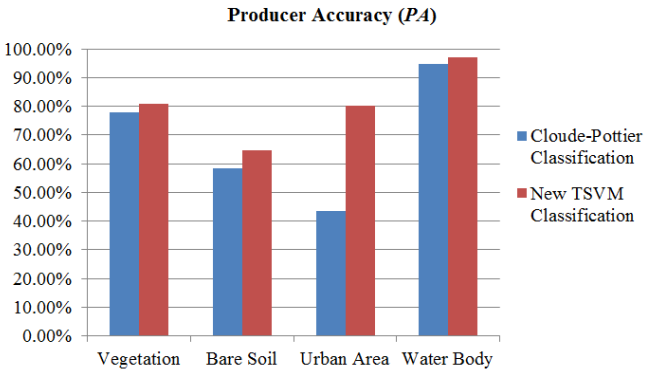

Fig. 6. *PA* of two classification methods over four land covers

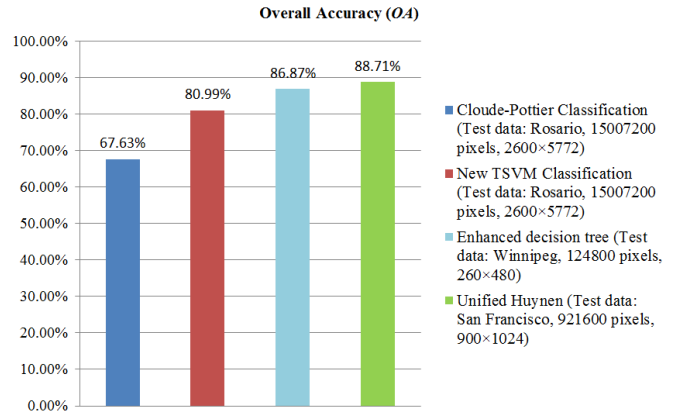

Fig. 7. OA of four classification methods

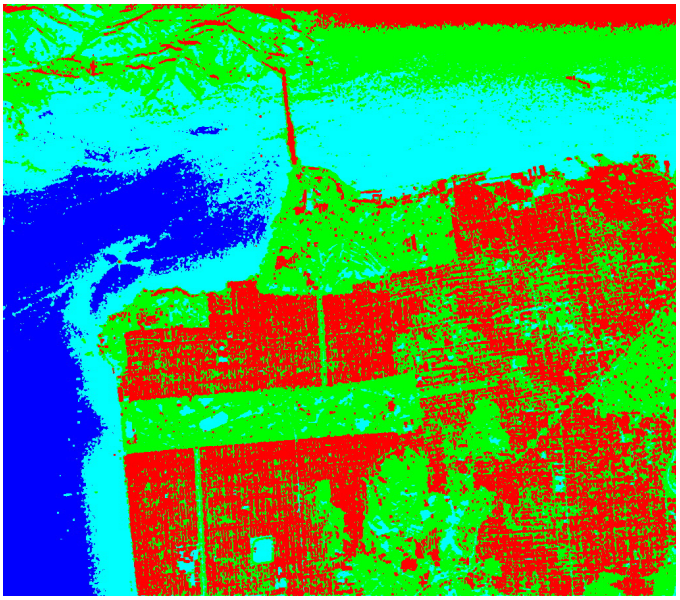

Fig. 8. Classification results evaluated on AIRSAR San Francisco data using the new proposed method. AIRSAR data courtesy NASA

V. Conclusion

The Touzi incoherent decomposition model allows a roll-invariant and unique target characterization. Hence, the Touzi scattering vector model is employed to extract coarse land classification maps in this study. A new unsupervised classifying scheme that incorporates the conventional Wishart statistical models is proposed based on the coarse land classification maps. Quantitative evaluation results validate the effectiveness of the new proposed method. Such sort of classifying method becomes even more important when it is impossible to acquire a large number of training samples with human annotations. In addition, it will be valuable to conduct a further revision to the TSVM model to improve the ability of discerning bare soil and conduct experiments on other airborne very high resolution PolSAR images.

Acknowledgment

The authors would like to thank the NASA for the provision of the UAVSAR data. The authors would also like to thank the European Space Agency (ESA) for the provision of the polarimetric SAR data processing and educational tool (PolSARPro). The authors would also like to thank the Prof. Touzi for his advice and Polarimetric Workstation (PWS) provided by the Canada Centre for Remote Sensing (CCRS). The authors would also like to thank Guangzhou Jiantong Surveying Mapping and Geo-information Technology Corporation for the production of ground truth data.

References

[1] S. Sun, R. Liu, and W. Wen, "Unsupervised Classification Method for Polarimetric Synthetic Aperture Radar Imagery Based on Yamaguchi Four-Component Decomposition Model," *Journal of Electrical and Computer Engineering*, 2015, Article ID 680715, 6 pages, Jun. 2015.

[2] S. Kusano, K. Takahashi, and M. Sato, "A New Decomposition of a POLSAR Coherency Matrix Using a Generalized Scattering Model," *IEEE Journal of Selected Topics in Applied Earth Observations and Remote Sensing*, vol. 8, no. 8, pp. 3933-3940, Aug. 2015.

[3] N. Besic, G. Vasile, J. Chanussot, and S. Stankovic, "Polarimetric Incoherent Target Decomposition by Means of Independent Component Analysis," *IEEE Transactions on Geoscience and Remote Sensing*, vol. 53, no. 3, pp. 1236-1247, Mar. 2015.

[4] A., Bhattacharya, G. Singh, S. Manickam, and Y. Yamaguchi, "An Adaptive General Four-Component Scattering Power Decomposition With Unitary Transformation of Coherency Matrix (AG4U)," *IEEE Geoscience and Remote Sensing Letters*, vol. 12, no. 10, pp. 2110-2114, Jul. 2015.

[5] Y. Yamaguchi, A. Sato, W.M. Boerner, R. Sato, and H. Yamada, "Four-Component Scattering Power Decomposition With Rotation of Coherency Matrix," *IEEE Transactions on Geoscience and Remote Sensing*, vol. 49, no. 6, pp. 2251-2258, Feb. 2011.

[6] R. Touzi, "Target Scattering Decomposition in Terms of Roll-Invariant Target Parameters," *IEEE Transactions on Geoscience and Remote Sensing*, vol. 45, no. 1, pp. 73-84, Dec. 2007.

[7] R. Touzi, "Polarimetric target scattering decomposition: A review," *in Proc. of the 2016 IEEE International Geoscience and Remote Sensing Symposium (IGARSS)*, Beijing, China, July 2016, pp. 5658-5661.

[8] B. H. Trisasongko, "Mapping stand age of rubber plantation using ALOS-2 polarimetric SAR data," *European Journal of Remote Sensing*, vol. 50, no. 1, pp. 64-76, Jan. 2017.

[9] R. Sonobe, Y. Yamaya, H. Tani, X. Wang, N. Kobayashi, and K. Mochizuki, "Assessing the suitability of data from Sentinel-1A and 2A for crop classification," *GIScience & Remote Sensing*, vol. 54, no. 6, pp. 918-938, Jul. 2017.

[10] S. Middinti, C. Jha, and T. Reddy, "Forest type classification with combination of advanced polarimetric decompositions and textures of L-band synthetic aperture radar data," *Journal of Applied Remote Sensing*, vol. 11, no. 1, pp. 016035, Mar. 2017.

[11] M. Ohki and M. Shimada, "Large-Area Land Use and Land Cover Classification With Quad, Compact, and Dual Polarization SAR Data by PALSAR-2," *IEEE Transactions on Geoscience and Remote Sensing*, vol. 56, no. 9, pp. 5550-5557, Sept. 2018.

[12] A. Buono, F. Nunziata, M. Migliaccio, X. Yang, and X. Li, "Classification of the Yellow River delta area using fully polarimetric SAR measurements," *International Journal of Remote Sensing*, vol.38, no.23, pp. 6714-6734, Aug. 2017.

[13] I. Khosravi, A. Safari, S. Homayouni, and H. McNairn, "Enhanced decision tree ensembles for land-cover mapping from fully polarimetric SAR data," *International Journal of Remote Sensing*, vol.38, no.23, pp. 7138-7160, Aug. 2017.

[14] D. Li and Y. Zhang, "Unified Huynen Phenomenological Decomposition of Radar Targets and Its Classification Applications," *IEEE Transactions on Geoscience and Remote Sensing*, vol. 54, no. 2, pp. 723-743, Feb. 2016.

[15] O. D'Hondt, S. Guillaso, and O. Hellwich, "Iterative Bilateral Filtering of Polarimetric SAR Data," *IEEE Journal of Selected Topics in Applied Earth Observations and Remote Sensing*, vol. 6, no. 3, pp. 1628-1639, Jun. 2013

[16] P. Rosen, S. Hensley, K. Wheeler, *et al.*, "UAVSAR: New NASA Airborne SAR System for Research," *IEEE Aerospace and Electronic Systems Magazine*, vol. 22, no. 11, pp. 21-28, Dec. 2007

[17] S. Sun, R. Liu, C. Yang, H. Zhou, J. Zhao, and J. Ma, "Comparative study on the speckle filters for the very high-resolution polarimetric synthetic aperture radar imagery," *Journal of Applied Remote Sensing*, vol. 10, no. 4, pp. 045014, Nov. 2016.

[18] J.W. Goodman, "Some fundamental properties of speckle," *Journal of the Optical Society of America*, vol. 66, no. 11, pp. 1145-1150, 1976.

[19] E. Pottier and J.S. Lee, "Unsupervised classification scheme of Polsar images based on the complex Wishart distribution and H/A/α polarimetric decomposition theorems," *in Proc. of the 3th European Conference on Synthetic Aperture Radar (EUSAR)*, Munich, Germany, May 2000, pp. 265-268.

[20] J.S. Lee, T. Ainsworth, Y. Wang, and K. Chen, "Polarimetric SAR Speckle Filtering and the Extended Sigma Filter," *IEEE Transactions on Geoscience and Remote Sensing*, vol. 53, no. 3, pp. 1150-1160, Mar. 2015

[21] R. Touzi, A. Deschamps, and R. Rother, "Phase of Target Scattering for Wetland Characterization Using Polarimetric C-Band SAR," *IEEE Transactions on Geoscience and Remote Sensing*, vol. 47, no. 9, pp. 3241-3261, Sept. 2009.

[22] X. Liu, L. Jiao, and F. Liu, "PolSF: PolSAR image dataset on San Francisco," arXiv preprint arXiv:1912.07259, 2019. Available: https://arxiv.org/abs/1912.07259